Analytical and Bioanalytical Chemistry (2022) 414:3827–3836
https://doi.org/10.1007/s00216-022-04024-4

RESEARCH PAPER

Ultrabright silicon nanoparticle fluorescence probe for sensitive detection of cholesterol in human serum

Xiwen Ye[1] · Yanxiao Jiang[2] · Xiaowei Mu[1] · Ying Sun[1] · Pinyi Ma[1] · Ping Ren[3] · Daqian Song[1]

Received: 8 February 2022 / Revised: 13 March 2022 / Accepted: 15 March 2022 / Published online: 26 March 2022

Abstract

A highly sensitive fluorescence-based assay for cholesterol detection was developed using water-dispersible green-emitting silicon nanoparticles (SiNPs) as a fluorescence indicator and enzyme-catalyzed oxidation product PPDox (Bandrowski's base) as a quencher. The SiNPs were facilely synthesized via a simple, one-step hydrothermal treatment using 3-[2-(2-aminoethylamino)ethylamino]propyl-trimethoxysilane (AEEA) as the silicon source, which has ultrahigh quantum yield and low phototoxicity. Under the catalysis of cholesterol oxidase (ChOx), hydrogen peroxide (H_2O_2) was generated as a result of cholesterol oxidation. Utilizing p-phenylenediamine (PPD) as the substrate for horseradish peroxidase (HRP) in the presence of H_2O_2 led to the production of PPDox. Based upon the inner filter effect (IFE), the established ultrasensitive fluorescent assay could accurately measure cholesterol. The limit of detection (LOD) of the assay was 0.018 μM with a linear range of 0.025–10 μM. The results for the detection of real serum samples by the proposed assay were comparable to those by a commercial reagent kit, demonstrating that our proposed strategy has high application potential in disease diagnosis and other related biological studies.

Keywords Cholesterol · Fluorescence · Silicon nanoparticles · Inner filter effect

Introduction

Cholesterol, the main steroid in mammals, is abundant in brain and nerve tissues. As an indispensable substance in cell metabolism, it not only is involved in the formation of cell membranes, but also acts as a precursor of other biomolecules such as bile acids, vitamin D, and steroid hormones [1, 2]. Generally, the normal level of cholesterol in human blood ranges from 2.83 to 5.20 mM [3]. The improper distribution or abnormal content of this lipid can lead to many serious diseases or disorders. Atherosclerosis, coronary heart disease, and cerebral thrombosis have been shown to be associated with an excessive level of the lipid [4, 5], while hypocholesterolemia, sepsis, and malnutrition have been demonstrated to be caused by a low concentration of the lipid [6]. Therefore, considering that cholesterol is an essential biomarker for numerous diseases, the ability to precisely monitor cholesterol concentration during the early diagnosis of the diseases can play a significant role in medical and clinical fields.

There are several strategies for detecting cholesterol, which include high performance liquid chromatography [7, 8], mass spectrometry [9], amperometric method [10, 11], colorimetry [12–14], electrochemistry [15, 16], electrochemiluminescence [17, 18], and fluorometry [19–21]; among which, fluorometry holds great advantages owing to its exceptional sensitivity, specificity, and instantaneity in sensing biomaterials after combining with fluorescent materials, which can be roughly divided into two categories: dyes and nanomaterials. Unlike most dyes that are synthesized intricately, nanomaterials contain noble metal nanoparticles, semiconductor nanocrystals,

✉ Pinyi Ma
mapinyi@jlu.edu.cn

✉ Ping Ren
rpemail@jlu.edu.cn

✉ Daqian Song
songdq@jlu.edu.cn

[1] Jilin Province Research Center for Engineering and Technology of Spectral Analytical Instruments, College of Chemistry, Jilin University, Qianjin Street 2699, Changchun 130012, China

[2] School of Marine Science and Technology, Harbin Institute of Technology at Weihai, Weihai 264209, Shandong, China

[3] Department of Thoracic Surgery, The First Hospital of Jilin University, Xinmin Street 71, Changchun 130021, China

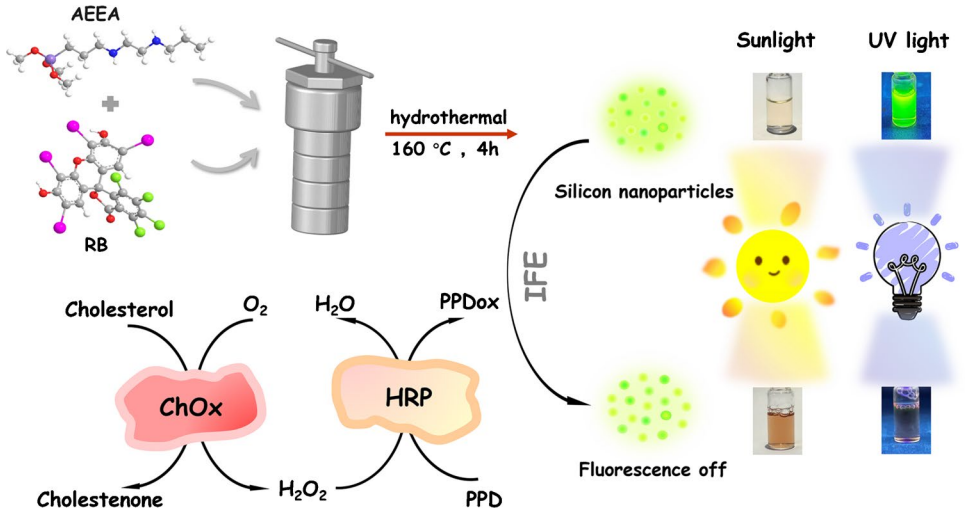

Scheme 1 Schematic illustration of cholesterol detection by the proposed nanoprobe

and carbon quantum dots which have been shown to be able to overcome drawbacks such as biological incompatibility, poor water solubility, and high toxicity [19, 22–25]. In addition, fluorescent silicon nanoparticles (SiNPs), as newly emerged nanomaterials, have particularly outstanding optical properties, superior quantum yield, robust photostability, and low cytotoxicity [26–28]. However, the utilization of SiNPs in bioanalysis or clinical diagnosis yet remains at an immature stage.

Herein, we established for the first time a sensitive fluorescent method for cholesterol detection using SiNPs as fluorescent probes and PPDox as a quencher. As shown in Scheme 1, the SiNPs were prepared using a facile hydrothermal method with superior quantum yield [29]. PPD, a chromogenic substrate, was finally converted into PPDox during two successive catalytic reactions, in which hydrogen peroxide was generated from cholesterol oxidation under the catalysis of cholesterol oxidase (ChOx) and from PPD oxidation induced by hydrogen peroxide under the catalysis of horseradish peroxidase (HRP). Because PPDox could suppress the emission of green fluorescence at 531 nm by absorbing the fluorescence via IFE mechanism; the fluorescence intensity of SiNPs was gradually restrained, thus allowing the ratio of fluorescence decrease (Rfd) to be used as the response signal in the detection of cholesterol. The proposed assay was applied to examine real and spiked human serum samples, and the results from which were in agreement with those examined using a commercial reagent kit, which further indicates the notable reliability and practicality of the proposed method.

Experimental sections

Chemical and biological reagents

3-[2-(2-Aminoethylamino)ethylamino]propyl-trimethoxysilane (AEEA) was purchased from Fluorochem Ltd. (Derbyshire, UK). Rose Bengal (RB), *p*-phenylenediamine (PPD), Triton X-100, D-(+)-galactose (Gal), L-phenylalanine (Phe), and bovine serum albumin (BSA) were supplied by Shanghai Aladdin Industrial Corporation. Tyrosine (Tyr) and D-(+)-xylose (Xyl) were purchased from Shanghai Macklin Biochemical Technology Co., Ltd. L-Leucine (Leu) and cholesterol were respectively from HuaYi Biotechnology Company Ltd. and Energy Chemical. ChOx, cholesterol esterase, and alkaline phosphate (ALP) were from Shanghai Yuanye Bio-Technology Co., Ltd. Horseradish peroxidase (HRP) and trilaurin (TG) were obtained from Beijing J&K Chemicals. Commercial total cholesterol content assay kit was supplied by Beijing Solarbio Science & Technology Co., Ltd. All the chemical reagents were of analytical grade and used without further purification. Ultrapure water with resistivity of 18.2 MΩ·cm at 25 °C prepared by a Milli-Q system (Millipore, USA) was used for all the syntheses and analyses. Aqueous solutions of cholesterol oxidase, HRP, and PPD were freshly prepared with BR buffer solution (0.04 M, pH = 8.0) before use.

Serum samples were collected from individual adult volunteers in the First Hospital of Jilin University (Changchun, China) and were diluted five 100-fold before analyses. Recovery experiments were performed with spiked serum samples.

Instruments

Fluorescence spectra were recorded on an F-2700 fluorescence spectrophotometer (Hitachi Ltd., Tokyo, Japan). UV–visible (UV–vis) absorption spectra were taken using a Cary 60 UV–vis absorption spectrometer (Agilent Technologies Inc., USA). Morphology of the SiNPs was characterized by a JEOL JEM-2100F transmission electron microscope (TEM, Japan) operated at 200 kV without staining. X-ray photoelectron spectroscopy (XPS) was obtained on

an ESCALAB 250 spectrometer (Thermo Fisher Scientific Inc., USA). Fourier transform infrared (FT-IR) absorption was measured on a Nicolet Avatar360 FT-IR spectrometer (Thermo Fisher Scientific Inc., USA). Fluorescence lifetime was performed on an FLS920 spectrometer (Edinburgh Instrument). An electric oven (Tianjin Taisite Instrument Co., Ltd., China) was employed for the hydrothermal reaction process. All pH values of buffer solutions were verified by a PHS-3C pH Meter (INESA Scientific Inc., China).

Synthesis of SiNPs

The fluorescent SiNPs used in the proposed assay were prepared by a facile one-pot hydrothermal method according to a previous report with some modifications [29]. Briefly, 60 mg of RB was dissolved in 8 mL of water. After 2 mL of AEEA was added, the mixture was transferred into a 30-mL Teflon-lined autoclave, which was then heated in an oven at 160 °C for 4 h. Subsequently, the resultant solution was dialyzed through a dialysis membrane (molecular weight cutoff of 500 Da) for 12 h to remove residual reagents. The final sample was stored at 4 °C until subsequent experiments. The prepared SiNPs were freshly diluted to 0.17 mg/mL before use.

Cholesterol measurement

Detection of cholesterol in a standard solution or a serum sample was carried out as follows. Firstly, 100 µL of BR buffer (pH = 8.0) solution, 100 µL of PPD (8 mM) solution, 100 µL of HRP (15 U/L) solution, 100 µL of ChOx (1000 U/L) solution, and 500 µL of cholesterol standard solution containing 1% Triton X-100 were successively added to a 2.0-mL microcentrifuge tube. After shaking gently, the mixture was incubated at 40 °C in the dark for 40 min. Then, 100 µL of diluted SiNPs was injected into the tube, and the mixture was shaken thoroughly. Finally, the obtained solution was transferred to a 1-cm quartz cuvette, in which its fluorescent spectrum was recorded at room temperature at an excitation wavelength of 490 nm.

For the assay of serum sample, 50 µL of cholesterol esterase was added to 500 µL of 500-fold diluted human serum, and the mixture was then incubated for 40 min. Other than replacing 100 µL of cholesterol oxidase (1000 U/L) solution with 50 µL of cholesterol oxidase (2000 U/L) solution, other procedures for the assay of total cholesterol in a real serum sample were the same as those used for standard solution. All experiments were carried out in triplicate.

In this work, the ratio of Rfd, which can indicate the efficiency of IFE, was calculated using the following formula.

$$\mathrm{Rfd} = \frac{F_0 - F}{F_0} \times 100\%$$

In the equation, F_0 and F are the fluorescence emission intensity of the blank sample and the standard (or real) sample, respectively.

Results and discussion

Characterization of the SiNPs

The morphological analysis of the prepared SiNPs showed that they have good dispersibility and uniform sizes with an average diameter of 2.5 nm (Fig. 1). The high-resolution TEM image (inset in Fig. 1a) exhibited the crystal lattice spacing of 0.32 nm, which was congruous with the lattice of Si(111), further confirming the crystallization of the SiNPs.

The FT-IR spectra indicated that there were functional groups attached to the surface of SiNPs (Fig. 2a). The peaks at 1315 cm^{-1} and 1123–1036 cm^{-1} attributed to the Si–C asymmetric deformation [30] and the Si–O–Si stretching vibration [31]. The peak appeared at 929 cm^{-1} was caused by the Si–O stretching vibration of the Si–OH group. The absorption bands at 3406 and 1636 cm^{-1} were derived from the O–H and C = O stretching vibrations. The characteristic

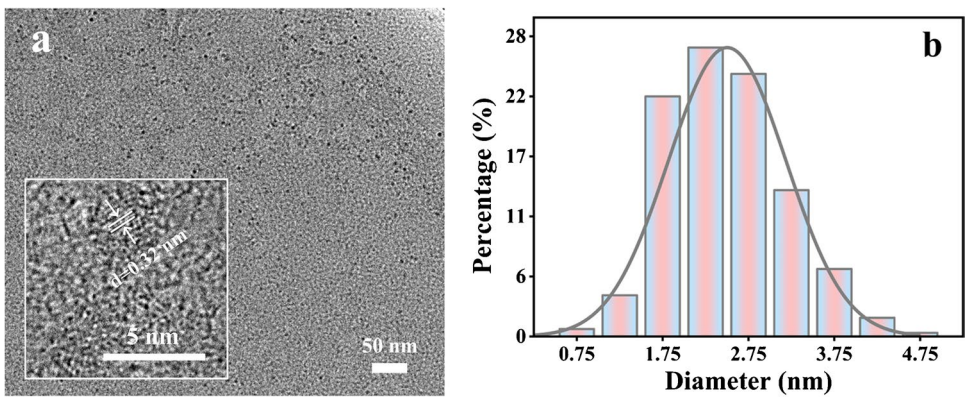

Fig. 1 **a** TEM image of SiNPs (inset is the lattice fringes). **b** Size distribution of SiNPs

absorption peaks at 2933 and 1474 cm^{-1} were due to the unsaturated stretching vibration and the bending vibration of the C–H bond. The characteristic absorption bands corresponding to the bending and wagging vibrations of N–H appeared at 1577 and 781 cm^{-1}. The band at 1384 cm^{-1} was assigned to the C–N stretching vibration. The peak at 691 cm^{-1} indicated the presence of secondary amine.

XPS measurements were performed to analyze the elemental composition of the prepared SiNPs (Fig. 2b–f). Five major peaks in the full-scan survey at 102 eV, 152 eV, 284 eV, 398 eV, and 531 eV represented Si 2p, Si 2 s, C 1 s, N 1 s, and O 1 s, respectively [32]. The high-resolution Si 2p spectrum revealed that there were three types of silicon atoms, including Si–C (101.3 eV/100.6 eV), Si–O–H (102.1 eV), and Si–O (103.3 eV) [33]. In the raw spectrum of O 1 s, three fitted peaks at 531.1 eV, 532.2 eV, and 531.6 eV were assigned to C = O, Si–O, and C = O/C–O–C, respectively [34]. The N 1 s signal could be fitted to three peaks at 398.7 eV, 401.2 eV, and 397.86 eV corresponding to C–N–C, C–NH_2, and Si–N, respectively [35]. The spectrum of C 1 s could be further divided into four peaks, including C–C/C = C (284.6 eV), C–Si (283.9 eV), C–OH/C–O–C (286.2 eV), and C = O (287.5 eV) [36]. These results were congruous with the FT-IR results.

Optical properties of the SiNPs

The optical properties of the SiNPs were examined using UV–vis absorption and fluorescence spectroscopy (Fig. 3a). The UV–vis absorption spectrum of SiNPs displayed a characteristic peak at 510 nm originated from the surface defect-induced trapping of the excited state. The SiNPs exhibited strong fluorescence emission at 531 nm under the excitation wavelength of 490 nm. In addition, the fluorescence emission wavelength remained constant as the excitation wavelength was varied from 430 to 510 nm, indicating that the SiNPs have size-independent emission characteristics (Figure S2a). The fluorescence quantum yield (QY) of the SiNPs measured in an aqueous solution reached up to 96.18%. The response of the SiNPs towards environmental pH adjusted by BR buffer was investigated (Figure S2b), and the results from which revealed that alkaline pH could benefit the fluorescence emission, which may be caused by the change of surface charge of SiNPs during deprotonation process. The salt tolerance (Figure S2c) and long-term photobleaching (Figure S2d) of the SiNPs were investigated seriatim. As can be seen, the irradiation at 490 nm for 60 min had little influence on the fluorescence emission of the SiNPs, indicating that they possess good stability, even when the concentration of NaCl solution was 100 mM.

Cholesterol-sensing mechanism

The oxidation of substrate, i.e., cholesterol through molecular O_2, by cholesterol oxidase generates H_2O_2 [37]. PPD, as an enzyme substrate, can be oxidized by HRP and H_2O_2 to PPDox (the oxidative product of PPD called Bandrowski's base, i.e., (3E,6E)-3,6-bis[(4-aminophenyl)imino]

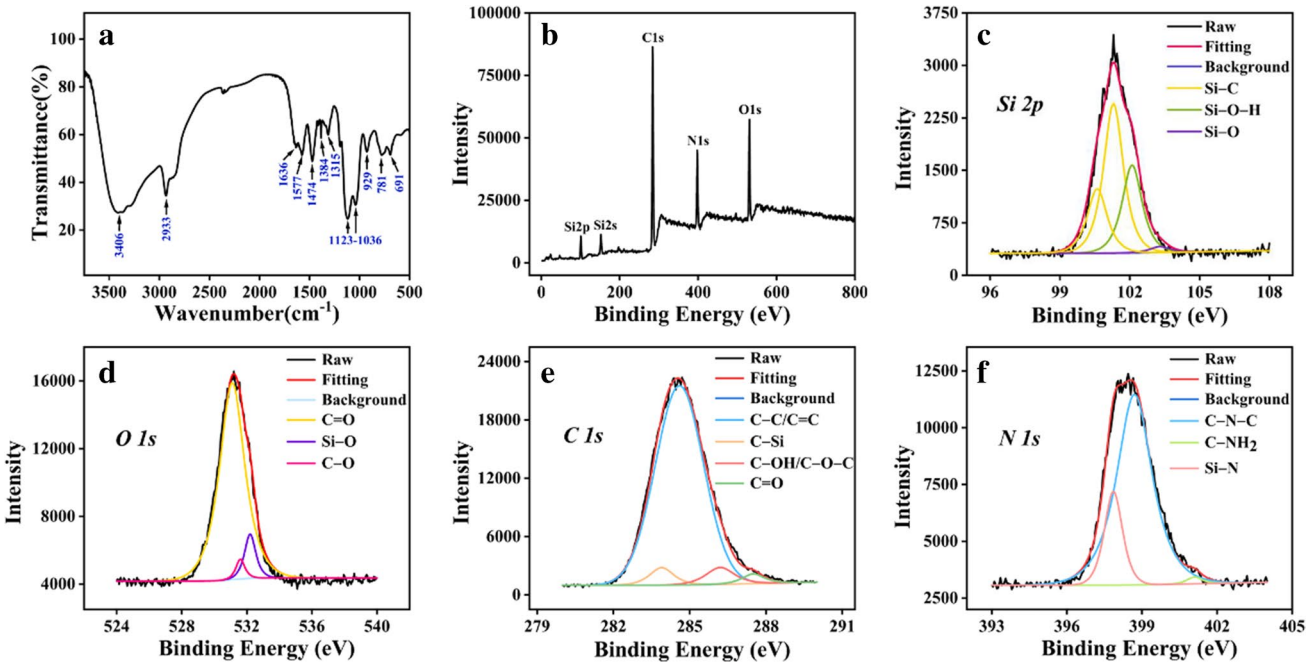

Fig. 2 **a** FT-IR spectrum of SiNPs. **b**—**f** High-resolution XPS spectra of **b** survey, **c** Si 2p, **d** O 1 s, **e** C 1 s, and **f** N 1 s

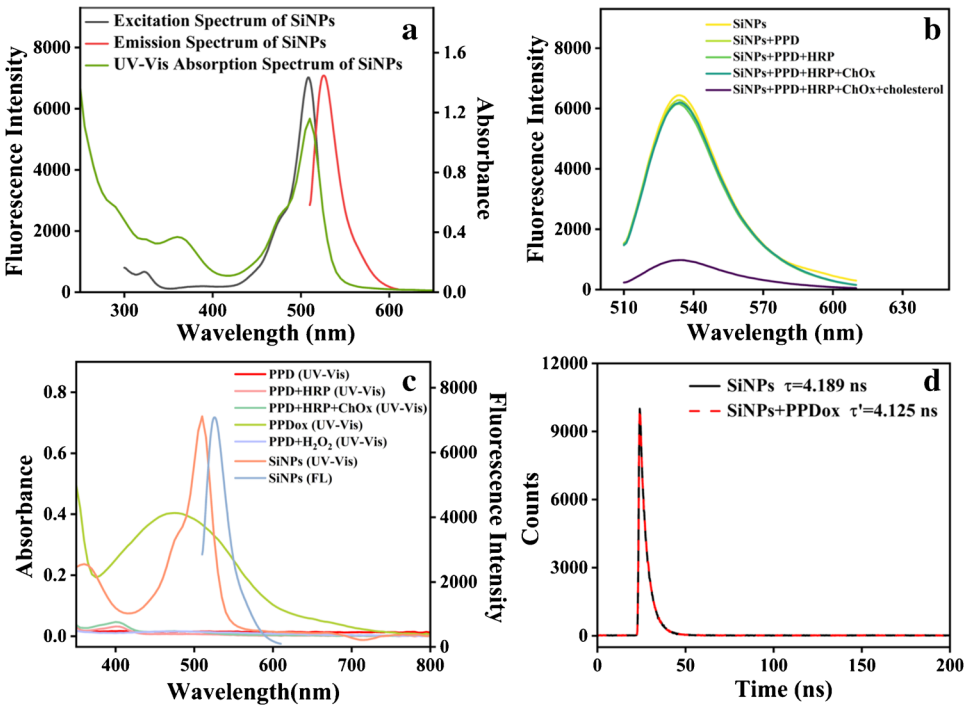

Fig. 3 **a** UV–vis absorption, fluorescence excitation, and fluorescence emission spectra of SiNPs. **b** Fluorescence variations of SiNPs in the presence of different substrates. **c** UV–vis absorption spectra of SiNPs, PPD and mixture of PPD coexisting with different substrates, and fluorescence emission spectrum of SiNPs. **d** Fluorescence lifetime of SiNPs in the absence and presence of PPDox

cyclohexa-1,4-diene-1,4-diamine) [38]. During the two continuous catalytic oxidation reactions, H_2O_2 acts as both the creation of the former reaction and the reactant of the latter reaction, while PPDox is the final product.

As shown in Fig. 3c, PPD did not exhibit obvious absorption peak in the presence of HRP or H_2O_2 alone, or in the copresence of HRP and ChOx. However, the absorbance peak of a mixture containing PPD, HRP, ChOx, and cholesterol was found obviously overlapped with the absorption band, as well as the fluorescence excitation and emission bands of SiNPs. It appears that PPDox was generated under the catalysis of HRP, and the production of PPDox could largely decrease the fluorescence emission of SiNPs.

The influences of PPD, HRP, ChOx, and cholesterol, as well as their combinations on the fluorescence of SiNPs were examined (Fig. 3b). Only the mixture consisting of PPD, HRP, ChOx, and cholesterol exhibited a conspicuous fluorescence quenching effect, which is consistent with the results described above.

The overlap between the absorption spectrum of the quencher (PPDox) and the excitation or emission spectrum of the fluorescent probe (SiNPs) suggests that the fluorescence quenching may be caused by either IFE or FRET. To further investigate the quenching mechanism, the fluorescence decay of the SiNPs was examined. Since FRET is a non-radiative energy transfer process, where the energy created by fluorescence excitation of the energy donor in its excited state is transferred to an adjacent energy acceptor, it leads to simultaneous fluorescence quenching and lifetime shortening of the donor [39]. However, IFE, which is the radiative energy transfer that results in the perturbation of the ground state of the fluorophores, contributes only to the quenching of the donor emission rather than the reduction of the fluorescence lifetime of fluorophores [40, 41]. As illustrated in Fig. 3d, the fluorescence lifetimes of SiNPs in the absence and presence of PPDox were 4.189 ns and 4.125 ns, respectively. As evidenced by the nearly unchanged values of the fluorescence lifetime in this assay, the quenching of fluorescence of SiNPs by PPDox may stem from IFE [42]. Theoretically, the IFE-based quenching of fluorophores by absorbers in the detection system relies on the absorption of the excitation or emission energy, or both simultaneously [43], and for this reason, the quenching efficiency varies with the excitation wavelength [44]. To further verify the IFE mechanism, the excitation wavelength-dependent fluorescence quenching behavior of the SiNPs was investigated (Figure S3). The results showed that the spectra of the excitation wavelength-dependent quenching of SiNPs resembled the absorption spectrum of the absorber PPDox, confirming the quenching mechanism described above.

Optimization of assay conditions

In order to obtain the optimal analytical performance, several experimental parameters involved in the proposed assay including pH value of BR buffer; temperature; incubation time; and concentrations of PPD, HRP, and ChOx were investigated (Figures S1a–f). The effect of pH range from 2.0 to 11.0 on the proposed method was determined. The ratio of fluorescence decrease gradually increased as the

pH value was increased from 2.0 to 8.0 and as highest at pH ~ 8.0, which may be arisen from the highest activity of HRP and ChOx. Further increasing the pH value to 11.0 caused a significant decrease of Rfd; thus, pH 8.0 was considered the optimal pH and was chosen in this assay. Reaction time and temperature are also important factors that can significantly influence the fluorescence intensity of the proposed method. The Rfd progressively increased with the increase of reaction time, was not obviously changed after 40 min, and reached its peak value at 40 °C. This indicates that the equilibrium was reached at 40 min, and the optimal temperature was 40 °C. Since the concentrations of PPD, HRP, and ChOx could also influence the dynamic detection range of the assay, these concentrations were also optimized and found to be optimal at 8 mM, 15 U/L, and 1000 U/L, respectively. These optimal concentrations were used in subsequent experiments.

Selectivity towards cholesterol of the nanoprobe

The meddling of several potential interferences including inorganic ions (Na^+, K^+, Mg^{2+}, and Ca^{2+}) and biomolecules (Gal, Tyr, TG, Xyl, Phe, Leu, ALP, GSH, Glu, Met, Ala, UA, and BSA) was evaluated. As can be seen in Fig. 4, these coexisting substances most hardly had influence upon the assay, just a few of them were slightly biased varying in degrees but barely affecting the results, indicating that the proposed assay has good selectivity for cholesterol.

Analytical performance

The fluorescence responses of the established assay to the changes of cholesterol concentrations are depicted in Fig. 5a. The fluorescence emission of the SiNPs steadily declined as the cholesterol concentration was continuously enhanced from 0 to 250 μM (Fig. 5b). The calibration curve of the assay was constructed by plotting the Rfd at 531 nm against the cholesterol concentration (Fig. 5c). The ratio of fluorescence decreased values was directly correlated with the increase of cholesterol concentration in the range of 0.025–10 μM. The detection limit (LOD) for the assay was calculated based on the value of three times the standard deviation (3σ) of the fluorescence response obtained from the blank sample and the slope (S) of the calibration curve, and was found to be 0.018 μM.

A comparison between the cholesterol-sensing performance of the proposed assay and that of other reported methods is presented in Table 1. The data adequately suggest that the proposed method is superior to other reported methods, owing to its lower LOD value, wider linear range, and higher sensitivity.

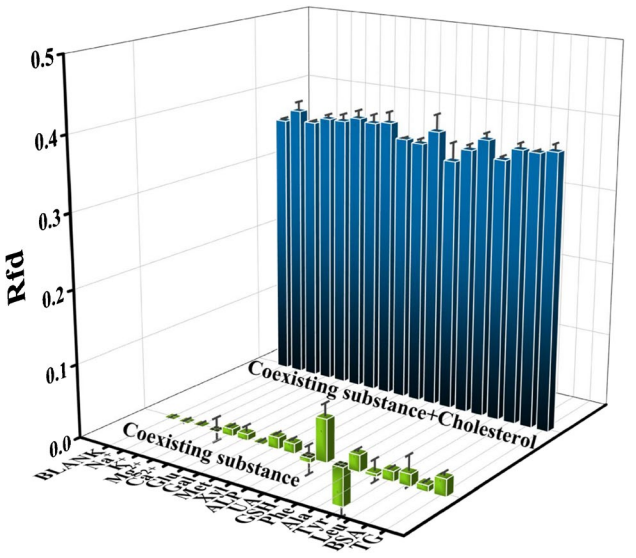

Fig. 4 Selectivity of the proposed assay towards cholesterol. Concentration of cholesterol was 7.5 μM. Concentrations of ALP and BSA were 50 U/L and 100 μg/L, respectively. Concentration of other interfering substances was 100 μM

Analysis of real samples

We further assessed the applicability of the proposed assay in detecting total cholesterol in clinical samples. The fabricated fluorometric approach and a commercial reagent kit were applied to detect real and spiked serum samples, and the results were compared (Fig. 6a, Table 2). There are two types of cholesterol in serum: free cholesterol and cholesterol ester, which together are called total cholesterol. The latter can be converted into free cholesterol by cholesterol esterase. Hence, the content of total cholesterol was determined via both cholesterol oxidase and cholesterol esterase. The recoveries were found ranging from 97 to 117% with a correlation coefficient (*r*), calculated based on the results from the two methods, of 0.997, showing the promising applicability of the method in rapid clinical diagnosis (Fig. 6b). Compared with that of the commercial reagent kit, which was between 0.156 and 5 mM, the linear range of this method was broader by three orders of magnitude. The content of cholesterol in human serum is at the level of millimoles per liter. The proposed assay was still able to detect it, despite being diluted by several thousand times. The dilution could reduce not only the concentration of cholesterol, but also the concentration of other coexisting substances. This process could greatly reduce the amount of latent interferences in the serum, thus improving the sensitivity of detection, endowing the method with enormous potential in diagnosis of samples with more complex environment.

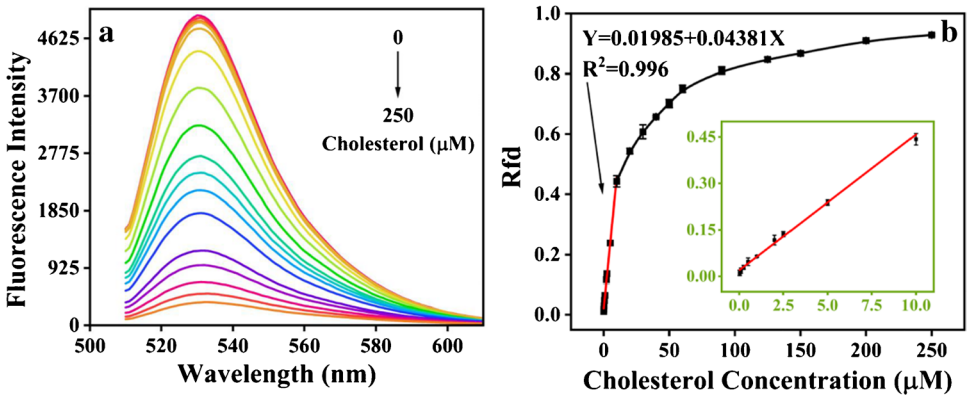

Fig. 5 **a** Fluorescence spectra of SiNPs upon the addition of cholesterol at various concentrations (from top to bottom: 0, 0.025, 0.1, 0.25, 0.5, 1, 2, 2.5, 5, 10, 15, 20, 25, 30, 35, 40, 45, 50, 60, 70, 80, 90, 100, 125, 150, 175, 200, and 250 μM). **b** Variation of fluorescence responses of the assay with increasing cholesterol concentration (Inset is a linear plot of Rfd versus cholesterol concentration from 0.025 to 10 μM)

Table 1 Comparison of analytical performance of this assay and other works for monitoring cholesterol

Method	Linear range (μM)	LOD (μM)	Ref
Gold nanocluster-assisted fluorometry	1–100	0.8	[45]
Carbon nitride quantum dot–based fluorometry	0–500	10.93	[46]
Carbon dots-cyanuric acid complex/MnO_2 nanosheet–based dual-emissive fluorescence and phosphorescence spectroscopy	67.89–5431.27	77.23	[47]
Enzyme-encapsulated MOF and AgNC/MoS2-NS nanocomposite–based fluorometry	0.06–15	0.03	[48]
Mo, S co-doped carbon quantum dot nanozyme-based cascade colorimetric spectroscopy	10–1000	7	[49]
MnO_2 nanosheets modified with 5-carboxyfluorescein-based fluorometry	1–300	0.33	[21]
SiNP-based fluorometry	0.025–10	0.018	This work

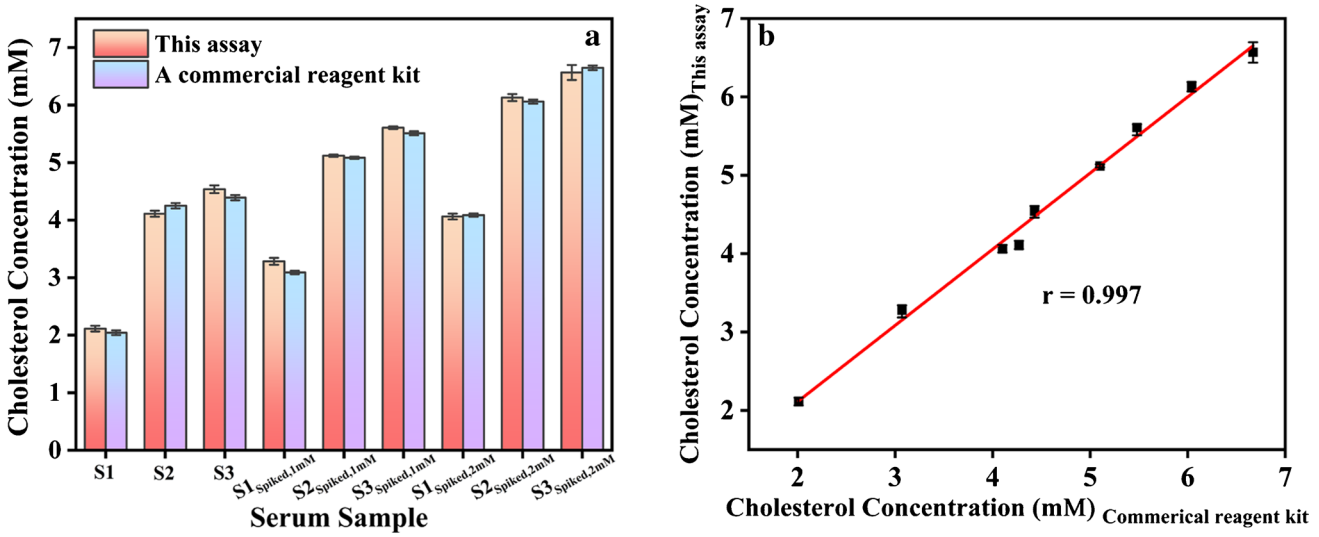

Fig. 6 **a** Comparison between quantification of cholesterol in real human serum samples by the proposed assay and that by a commercial reagent kit. **b** Correlation between cholesterol concentrations detected by the two methods

Conclusions

In summary, we developed a new IFE-based fluorescent assay for cholesterol detection using SiNPs as a fluorescent indicator. Since H_2O_2 could act as a vital link between two enzyme-catalyzed oxidation reactions, PPDox, which is both the final product and an IFE absorber, could distinctly absorb the green-light fluorescence of SiNPs. Through the observation of fluorescence variation during sensing, the developed assay was found to have strikingly high

Table 2 Detection of cholesterol in real and spiked human serum samples by this assay and a commercial reagent kit ($n=3$)

Serum sample	Spiked (mM)	This assay			Commercial reagent kit		
		Detected (mM)	Recovery (%)	RSD ($n=3$, %)	Detected (mM)	Recovery (%)	RSD ($n=3$, %)
S1	0	2.11 ± 0.051	-	2.42	2.01 ± 0.007	-	0.35
	1	3.28 ± 0.058	117.0	1.78	3.07 ± 0.018	106.5	0.58
	2	4.06 ± 0.052	97.4	1.27	4.10 ± 0.029	104.5	0.70
S2	0	4.11 ± 0.056	-	1.35	4.27 ± 0.019	-	0.44
	1	5.12 ± 0.020	100.9	0.38	5.10 ± 0.008	82.4	0.16
	2	6.13 ± 0.057	101.0	0.94	6.04 ± 0.015	88.2	0.24
S3	0	4.54 ± 0.071	-	1.57	4.43 ± 0.008	-	0.18
	1	5.61 ± 0.023	107.1	0.41	5.48 ± 0.029	104.6	0.52
	2	6.57 ± 0.126	101.4	1.91	6.67 ± 0.004	112.0	0.06

The detected results were the mean of three parallel measurements ± standard deviation (SD).

Recovery (%) = [(detected value − blank value)/added value] × 100%, the blank value was the value of unspiked sample.

RSD (%) = (SD/mean) × 100%

analytical performance, including a broad linear range and a very low LOD. Additionally, the cholesterol detection results obtained by the proposed assay were found to have good correlation with those obtained by a commercial reagent kit. Further comparison of the performance of the present method with that of other spectroscopic methods reported in the literature indicated that the present method could have a great potential in disease diagnosis and bioanalysis.

Supplementary Information The online version contains supplementary material available at https://doi.org/10.1007/s00216-022-04024-4.

Author contribution All authors have given approval for the final version of the paper.

Funding This work was supported by the National Natural Science Foundation of China (Grant Nos. 22074052 and 22004046).

Declarations

Ethics approval All applicable international, national, and/or institutional guidelines for the collection and use of human blood and serum samples were followed. The study was approved by the Institutional Ethics Committee of the First Hospital of Jilin University, Changchun, China.

Competing interests The authors declare no competing interests.

References

1. Maxfield FR, Tabas I. Role of cholesterol and lipid organization in disease. Nature. 2005;438(7068):612–21. https://doi.org/10.1038/nature04399.
2. Devadoss A, Burgess JD. Steady-state detection of cholesterol contained in the plasma membrane of a single cell using lipid bilayer-modified microelectrodes incorporating cholesterol oxidase. J Am Chem Soc. 2004;126(33):10214–5. https://doi.org/10.1021/ja047856e.
3. Amiri M, Arshi S. An overview on electrochemical determination of cholesterol. Electroanalysis. 2020;32(7):1391–407. https://doi.org/10.1002/elan.201900669.
4. Sekretaryova AN, Beni V, Eriksson M, Karyakin AA, Turner AP, Vagin MY. Cholesterol self-powered biosensor. Anal Chem. 2014;86(19):9540–7. https://doi.org/10.1021/ac501699p.
5. Blood cholesterol and vascular mortality by age, sex, and blood pressure: a meta-analysis of individual data from 61 prospective studies with 55 000 vascular deaths (2007). The Lancet 370 (9602):1829–1839. https://doi.org/10.1016/s0140-6736(07)61778-4
6. Huang S, Yang E, Yao J, Chu X, Liu Y, Zhang Y, Xiao Q. Nitrogen, cobalt co-doped fluorescent magnetic carbon dots as ratiometric fluorescent probes for cholesterol and uric acid in human blood serum. ACS Omega. 2019;4(5):9333–42. https://doi.org/10.1021/acsomega.9b00874.
7. Sinha A, Basiruddin S, Chakraborty A, Jana NR. beta-Cyclodextrin functionalized magnetic mesoporous silica colloid for cholesterol separation. ACS Appl Mater Interfaces. 2015;7(2):1340–7. https://doi.org/10.1021/am507817b.
8. Ronsein GE, Prado FM, Mansano FV, Oliveira MCB, Medeiros MHG, Miyamoto S, Di Mascio P. Detection and characterization of cholesterol-oxidized products using HPLC coupled to dopant assisted atmospheric pressure photoionization tandem mass spectrometry. Anal Chem. 2010;82(17):7293–301. https://doi.org/10.1021/ac1011987.
9. Houdová D, Soto J, Castro R, Rodrigues J, Soledad Pino-González M, Petković M, Bandosz TJ, Algarra M. Chemically heterogeneous carbon dots enhanced cholesterol detection by MALDI TOF mass spectrometry. J Colloid Interface Sci. 2021;591:373–83. https://doi.org/10.1016/j.jcis.2021.02.004.
10. Devadoss A, Burgess JD. Detection of cholesterol through electron transfer to cholesterol oxidase in electrode-supported lipid bilayer membranes. Langmuir. 2002;18(25):9617–21. https://doi.org/10.1021/la0258594.
11. Dey RS, Raj CR. Development of an amperometric cholesterol biosensor based on graphene−Pt nanoparticle hybrid material. The Journal of Physical Chemistry C. 2010;114(49):21427–33. https://doi.org/10.1021/jp105895a.
12. Zhao M, Li Y, Ma X, Xia M, Zhang Y. Adsorption of cholesterol oxidase and entrapment of horseradish peroxidase in

metal-organic frameworks for the colorimetric biosensing of cholesterol. Talanta. 2019;200:293–9. https://doi.org/10.1016/j.talanta.2019.03.060.
13. Nirala NR, Pandey S, Bansal A, Singh VK, Mukherjee B, Saxena PS, Srivastava A. Different shades of cholesterol: gold nanoparticles supported on MoS2 nanoribbons for enhanced colorimetric sensing of free cholesterol. Biosens Bioelectron. 2015;74:207–13. https://doi.org/10.1016/j.bios.2015.06.043.
14. Kitchawengkul N, Prakobkij A, Anutrasakda W, Yodsin N, Jungsuttiwong S, Chunta S, Amatatongchai M, Jarujamrus P. Mimicking peroxidase-like activity of nitrogen-doped carbon dots (N-CDs) coupled with a laminated three-dimensional microfluidic paper-based analytical device (laminated 3D-muPAD) for smart sensing of total cholesterol from whole blood. Anal Chem. 2021;93(18):6989–99. https://doi.org/10.1021/acs.analchem.0c05459.
15. Maduraiveeran G, Sasidharan M, Ganesan V. Electrochemical sensor and biosensor platforms based on advanced nanomaterials for biological and biomedical applications. Biosens Bioelectron. 2018;103:113–29. https://doi.org/10.1016/j.bios.2017.12.031.
16. Thakur N, Kumar M, Das Adhikary S, Mandal D, Nagaiah TC. PVIM-Co5POM/MNC composite as a flexible electrode for the ultrasensitive and highly selective non-enzymatic electrochemical detection of cholesterol. Chem Commun (Camb). 2019;55(34):5021–4. https://doi.org/10.1039/c9cc01534e.
17. Wu X, Chai Y, Yuan R, Zhong X, Zhang J. Synthesis of multiwall carbon nanotubes-graphene oxide-thionine-Au nanocomposites for electrochemiluminescence detection of cholesterol. Electrochim Acta. 2014;129:441–9. https://doi.org/10.1016/j.electacta.2014.02.103.
18. Xu J, Jiang D, Qin Y, Xia J, Jiang D, Chen HY. C3N4 nanosheet modified microwell array with enhanced electrochemiluminescence for total analysis of cholesterol at single cells. Anal Chem. 2017;89(4):2216–20. https://doi.org/10.1021/acs.analchem.6b04635.
19. Mir IA, Kumar S, Bhat MA, Yuelin X, Wani AA, Zhu L (2021) Core@shell quantum dots as a fluorescent probe for the detection of cholesterol and heavy metal ions in aqueous media. Colloids and Surfaces A: Physicochemical and Engineering Aspects 626. https://doi.org/10.1016/j.colsurfa.2021.127090
20. Li J, Liu T, Liu S, Li J, Huang G, Yang HH. Bifunctional magnetic nanoparticles for efficient cholesterol detection and elimination via host-guest chemistry in real samples. Biosens Bioelectron. 2018;120:137–43. https://doi.org/10.1016/j.bios.2018.08.046.
21. Han T, Zhu S, Wang S, Wang B, Zhang X, Wang G. Fluorometric methods for determination of H2O2, glucose and cholesterol by using MnO2 nanosheets modified with 5-carboxyfluorescein. Mikrochim Acta. 2019;186(5):269. https://doi.org/10.1007/s00604-019-3381-1.
22. Li D, Qiao Z, Yu Y, Tang J, He X, Shi H, Ye X, Lei Y, Wang K. In situ fluorescence activation of DNA-silver nanoclusters as a label-free and general strategy for cell nucleus imaging. Chem Commun (Camb). 2018;54(9):1089–92. https://doi.org/10.1039/c7cc08228b.
23. Xu F, Shi H, He X, Wang K, He D, Guo Q, Qing Z, Yan L, Ye X, Li D, Tang J. Concatemeric dsDNA-templated copper nanoparticles strategy with improved sensitivity and stability based on rolling circle replication and its application in microRNA detection. Anal Chem. 2014;86(14):6976–82. https://doi.org/10.1021/ac500955r.
24. Ma C, Bian T, Yang S, Liu C, Zhang T, Yang J, Li Y, Li J, Yang R, Tan W. Fabrication of versatile cyclodextrin-functionalized upconversion luminescence nanoplatform for biomedical imaging. Anal Chem. 2014;86(13):6508–15. https://doi.org/10.1021/ac5010103.
25. Xia T, Liu G, Wang J, Hou S, Hou S. MXene-based enzymatic sensor for highly sensitive and selective detection of cholesterol. Biosens Bioelectron. 2021;183: 113243. https://doi.org/10.1016/j.bios.2021.113243.
26. Li Q, Luo TY, Zhou M, Abroshan H, Huang J, Kim HJ, Rosi NL, Shao Z, Jin R. Silicon nanoparticles with surface nitrogen: 90% quantum yield with narrow luminescence bandwidth and the ligand structure based energy law. ACS Nano. 2016;10(9):8385–93. https://doi.org/10.1021/acsnano.6b03113.
27. Phan LMT, Baek SH, Nguyen TP, Park KY, Ha S, Rafique R, Kailasa SK, Park TJ. Synthesis of fluorescent silicon quantum dots for ultra-rapid and selective sensing of Cr(VI) ion and biomonitoring of cancer cells. Mater Sci Eng C Mater Biol Appl. 2018;93:429–36. https://doi.org/10.1016/j.msec.2018.08.024.
28. Zhong Y, Sun X, Wang S, Peng F, Bao F, Su Y, Li Y, Lee S-T, He Y. Facile, large-quantity synthesis of stable, tunable-color silicon nanoparticles and their application for long-term cellular imaging. ACS Nano. 2015;9(6):5958–67. https://doi.org/10.1021/acsnano.5b00683.
29. Chen X, Zhang X, Xia L-Y, Wang H-Y, Chen Z, Wu F-G. One-step synthesis of ultrasmall and ultrabright organosilica nanodots with 100% photoluminescence quantum yield: long-term lysosome imaging in living, fixed, and permeabilized cells. Nano Lett. 2018;18(2):1159–67. https://doi.org/10.1021/acs.nanolett.7b04700.
30. Han Y, Chen Y, Feng J, Liu J, Ma S, Chen X. One-pot synthesis of fluorescent silicon nanoparticles for sensitive and selective determination of 2,4,6-trinitrophenol in aqueous solution. Anal Chem. 2017;89(5):3001–8. https://doi.org/10.1021/acs.analchem.6b04509.
31. Ma SD, Chen YL, Feng J, Liu JJ, Zuo XW, Chen XG. One-step synthesis of water-dispersible and biocompatible silicon nanoparticles for selective heparin sensing and cell imaging. Anal Chem. 2016;88(21):10474–81. https://doi.org/10.1021/acs.analchem.6b02448.
32. Geng X, Li Z, Hu Y, Liu H, Sun Y, Meng H, Wang Y, Qu L, Lin Y. One-pot green synthesis of ultrabright N-doped fluorescent silicon nanoparticles for cellular imaging by using ethylenediaminetetraacetic acid disodium salt as an effective reductant. ACS Appl Mater Interfaces. 2018;10(33):27979–86. https://doi.org/10.1021/acsami.8b09242.
33. Lillo CR, Romero JJ, Portolés ML, Diez RP, Caregnato P, Gonzalez MC. Organic coating of 1–2-nm-size silicon nanoparticles: effect on particle properties. Nano Res. 2015;8(6):2047–62. https://doi.org/10.1007/s12274-015-0716-z.
34. Na M, Chen Y, Han Y, Ma S, Liu J, Chen X. Determination of potassium ferrocyanide in table salt and salted food using a water-soluble fluorescent silicon quantum dots. Food Chem. 2019;288:248–55. https://doi.org/10.1016/j.foodchem.2019.02.111.
35. Na M, Han Y, Chen Y, Ma S, Liu J, Chen X. Synthesis of silicon nanoparticles emitting yellow-green fluorescence for visualization of pH change and determination of intracellular pH of living cells. Anal Chem. 2021;93(12):5185–93. https://doi.org/10.1021/acs.analchem.0c05107.
36. Han Y, Chen Y, Feng J, Na M, Liu J, Ma Y, Ma S, Chen X. Investigation of nitrogen content effect in reducing agent to prepare wavelength controllable fluorescent silicon nanoparticles and its application in detection of 2-nitrophenol. Talanta. 2019;194:822–9. https://doi.org/10.1016/j.talanta.2018.11.008.
37. MacLachlan J, Wotherspoon ATL, Ansell RO, Brooks CJW. Cholesterol oxidase: sources, physical properties and analytical applications. J Steroid Biochem Mol Biol. 2000;72(5):169–95. https://doi.org/10.1016/S0960-0760(00)00044-3.
38. Zhang Y, Schmid YRF, Luginbuhl S, Wang Q, Dittrich PS, Walde P. Spectrophotometric quantification of peroxidase with

p-phenylenediamine for analyzing peroxidase-encapsulating lipid vesicles. Anal Chem. 2017;89(10):5484–93. https://doi.org/10.1021/acs.analchem.7b00423.
39. Xiong J, He S, Wang Z, Xu Y, Zhang L, Zhang H, Jiang H. Dual-readout fluorescence quenching immunochromatographic test strips for highly sensitive simultaneous detection of chloramphenicol and amantadine based on gold nanoparticle-triggered photoluminescent nanoswitch control. J Hazard Mater. 2022;429:128316. https://doi.org/10.1016/j.jhazmat.2022.128316.
40. Zhang J, Zhou R, Tang D, Hou X, Wu P. Optically-active nanocrystals for inner filter effect-based fluorescence sensing: achieving better spectral overlap. TrAC, Trends Anal Chem. 2019;110:183–90. https://doi.org/10.1016/j.trac.2018.11.002.
41. Ni P, Chen C, Jiang Y, Zhang C, Wang B, Lu Y, Wang H (2020) A fluorescent assay for alkaline phosphatase activity based on inner filter effect by in-situ formation of fluorescent azamonardine. Sensors and Actuators B: Chemical 302. https://doi.org/10.1016/j.snb.2019.127145
42. Mu X, Wu M, Zhang B, Liu X, Xu S, Huang Y, Wang X, Song D, Ma P, Sun Y (2021) A sensitive "off-on" carbon dots-Ag nanoparticles fluorescent probe for cysteamine detection via the inner filter effect. Talanta 221. https://doi.org/10.1016/j.talanta.2020.121463
43. Wang HB, Tao BB, Wu NN, Zhang HD, Liu YM. Glutathione-stabilized copper nanoclusters mediated-inner filter effect for sensitive and selective determination of p-nitrophenol and alkaline phosphatase activity. Spectrochim Acta A Mol Biomol Spectrosc. 2022;271: 120948. https://doi.org/10.1016/j.saa.2022.120948.
44. Zhang J, Lu X, Lei Y, Hou X, Wu P. Exploring the tunable excitation of QDs to maximize the overlap with the absorber for inner filter effect-based phosphorescence sensing of alkaline phosphatase. Nanoscale. 2017;9(40):15606–11. https://doi.org/10.1039/c7nr03673f.
45. Chang HC, Ho JA. Gold nanocluster-assisted fluorescent detection for hydrogen peroxide and cholesterol based on the inner filter effect of gold nanoparticles. Anal Chem. 2015;87(20):10362–7. https://doi.org/10.1021/acs.analchem.5b02452.
46. Chen Y, Yang G, Gao S, Zhang L, Yu M, Song C, Lu Y. Highly rapid and non-enzymatic detection of cholesterol based on carbon nitride quantum dots as fluorescent nanoprobes. RSC Adv. 2020;10(65):39596–600. https://doi.org/10.1039/d0ra07495k.
47. Su Q, Gan L, Zhu Y, Yang X (2021) Dual-emissive fluorescence and phosphorescence detection of cholesterol and glucose based on carbon dots-cyanuric acid complex quenched by MnO2 nanosheets. Sensors and Actuators B: Chemical 335. https://doi.org/10.1016/j.snb.2021.129715
48. Hassanzadeh J, Khataee A, Eskandari H. Encapsulated cholesterol oxidase in metal-organic framework and biomimetic Ag nanocluster decorated MoS2 nanosheets for sensitive detection of cholesterol. Sens Actuators, B Chem. 2018;259:402–10. https://doi.org/10.1016/j.snb.2017.12.068.
49. Zhao L, Wu Z, Liu G, Lu H, Gao Y, Liu F, Wang C, Cui J, Lu G. High-activity Mo, S co-doped carbon quantum dot nanozyme-based cascade colorimetric biosensor for sensitive detection of cholesterol. J Mater Chem B. 2019;7(44):7042–51. https://doi.org/10.1039/c9tb01731c.